Dynamic modelling of a UK North Sea saline formation for CO_2 sequestration

Francesca E. Watson, Simon A. Mathias, Susie E. Daniels, Richard R. Jones, Richard J. Davies, Ben J. Hedley, Jeroen van Hunen

Abstract

Preliminary dynamic modelling, using TOUGH2/ECO2N, has been carried out to assess the suitability of a site in the UK North Sea for sequestering CO_2. The potential storage site is a previously unused saline formation within the Permian Rotliegend sandstone. Data regarding the site is limited. Therefore, additional input parameters for the model have been taken from the literature and nearby analogues. The sensitivity of the model to a range of parameters has been tested. Results indicate that the site can sustain an injection rate of around 2.5 Mt a^{-1} of CO_2 for 20 years. The main control on pressure buildup in the model is the permeability of the unit directly beneath the Rotliegend in the location of the proposed storage site. The plume diameter is primarily controlled by the porosity and permeability of the site. A comparison between static, analytical and dynamic modelling highlights the advantages of dynamic modelling for a study such as this. Further data collection and modelling is required to improve predictions of pressure buildup and CO_2 migration. Despite uncertainties in the input data, the use of a full 3D numerical simulation has been extremely useful for identifying and prioritising factors which need further investigation.

Keywords:

Carbon sequestration, CO_2, dynamic modelling, UK North Sea, saline formation, greenhouse gas, global warming, climate change

Carbon sequestration has been proposed as a method of keeping atmospheric greenhouse gas emissions at an acceptable level (Pacala and Socolow 2004). Deep saline formations are one possible storage option for CO_2 as they contain large volumes of pore space and are regionally extensive (IPCC 2005). One of the advantages of using previously unused saline formations for CO_2 storage is the fact that they may have a reduced well density compared with oil or gas fields. Therefore, the number of man made leakage pathways is reduced. This is also a disadvantage as it means that there is limited data available about the formation for site-scale characterisation.

The EU directive (European Union 2009) requires the screening of a range of sites in order to identify those which are promising for CO_2 storage. Potential storage sites, chosen from preliminary screening, then need to be fully characterised using static and dynamic computer simulations which should demonstrate storage capacity, pressure buildup and CO_2 migration pathways. A site can only

be used for CO_2 storage if the site characterisation indicates that the risk of CO_2 leakage is insignificant and that there are no significant risks to human health or the environment.

This paper describes a preliminary site characterisation, undertaken for a deep saline formation in the North Sea, using a very limited dataset. This comes after the regional screening stage but is prior to the full site characterisation stage of the CO_2 storage workflow described above. The aim of the work is to build a dynamic model with which to assess the potential for CO2 storage at the proposed site and to identify further data which will be needed before a thorough site assessment can be carried out.

The site being considered for CO_2 storage is located in the Central North Sea (Fig. 1(a)). It is 50 km west of the Central Graben and 70km north of the Mid North Sea High, on the south western edge of the Northern Permian Basin. This is approximately 200 km North East of the UK Teesside industrial processing region which could provide the source of CO_2. The potential storage formation is the Permian Rotliegend Sandstone with the Permian Zechstein Salt providing the cap rock (Glennie 1983).

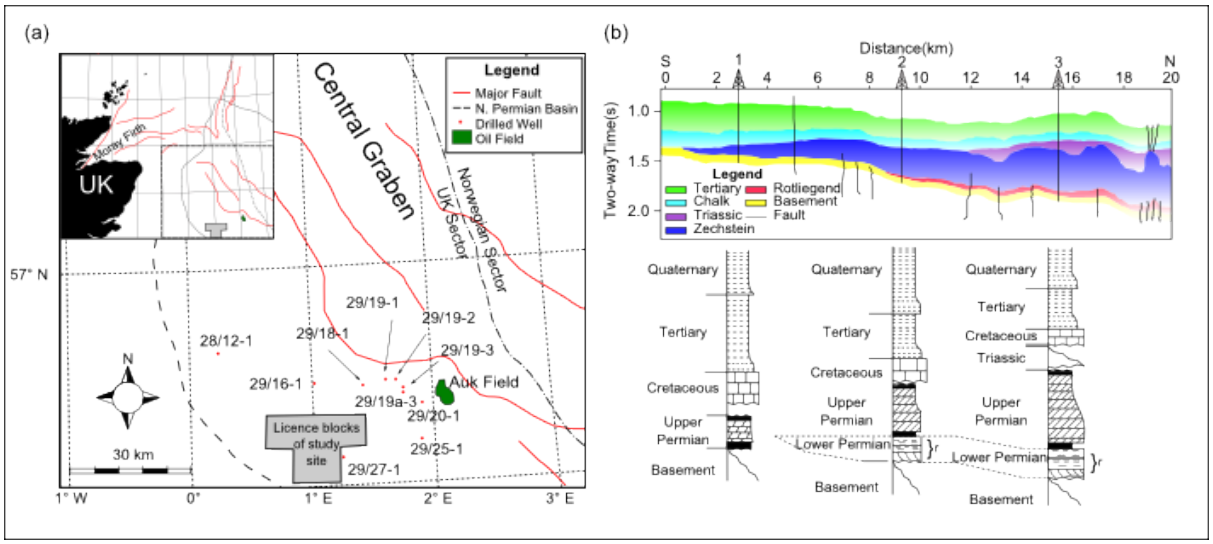

Fig. 1. (a) *Location map of the study site showing wells logs used in this study.* ***(b)*** *Regional structure and stratigraphy based on regional seismic line. Schematic wells show lateral variations in unit thickness. The reservoir interval is denoted (r). After Hedley et al. (2013).*

The intended preliminary trap within the Rotliegend is referred to hereafter as the CCC Prospect. A 2D seismic survey carried out over the proposed storage site shows that the CCC Prospect consists of a series of interconnected four-way dip closures. It is known that the Rotliegend pinches out to the south west of the site about 30 km away from the CCC Prospect (Fig. 1(b)). As the pinchout is updip from the CCC Prospect it could form a secondary trap in the event of CO_2 escaping from the CCC site.

CO_2 storage in saline formations in the UK North Sea

In order to meet emissions reductions targets the UK may need to store between 2 and 5 billion tonnes of CO_2 before 2050. The Department for Energy and Climate Change estimated that the UK has the potential to store 60 billion tonnes of CO_2 within saline formations in the UK North Sea and the East Irish Sea (DECC 2012). However, this storage capacity is not well understood and requires further investigation before storage operations can begin.

Formations within the North Sea have proven ability to store CO_2 both in natural accumulations (Yielding *et al.* 2011) and as part of a large scale carbon sequestration project (Chadwick *et al.* 2009b; Boait *et al.* 2012). Currently there is no injection of CO_2 for storage purposes within the UK North Sea.

Most previously published work regarding CO_2 storage in specific saline formations in the UK North Sea has been associated with the Triassic Bunter Sandstone Formation, within the Southern North Sea. Bentham *et al.* (2006) estimated the total storage capacity for several structures within the Bunter Sandstone based on their pore volume, CO_2 density at reservoir conditions and a factor representing the proportion of porespace likely to be filled with with CO_2. This factor was derived from a numerical model of a planned CO_2 injection into the Esmond field in the Bunter Sandstone. These estimates were mostly constrained by plume geometry and did not include the potentially limiting effect of pressure buildup on CO_2 injection.

Heinemann *et al.* (2012) estimated the dynamic storage capacity of the Bunter Sandstone by approximating it as a series of identical unit cells each containing an injection well at its centre. The minimum allowable well spacing was determined by finding the minimum cell size where the pressure increase due to injection stayed below some maximum pressure threshold. Estimates calculated in this way, which include the impact of pressure buildup on injection, were 2 – 4 times smaller than the static estimates given by Bentham *et al.* (2006). Noy *et al.* (2012) modelled a 113 km x 160 km portion of the Bunter Sandstone and estimate that 15 – 20 Mt a^{-1} could be stored in it over a 50 year period.

As part of the CASSEM (CO_2 Aquifer Storage Site Evaluation and Monitoring) project two onshore analogues for potential offshore CO_2 storage sites were modelled (Jin *et al.* 2010). The analogues chosen were the Kinniswood and Knox Pulpit Formations, in the east of Scotland and the Triassic Sherwood Sandstone in the east of England, the second of which is very similar to the Bunter Sandstone. The aim of the CASSEM project was to consider and refine the methods used for site characterisation as opposed to investigating the storage potential of any particular sites. However, they calculated storage efficiencies (the maximum volume of CO_2 stored divided by the total pore volume of the storage site) for the two sites at between 0.46 % and 2.75 %. These efficiencies led to storage capacity estimates of 800 Mt and 2300 Mt which indicate the potential for CO_2 storage at similar sites in the UK North Sea.

Our work investigates the potential pressure buildup and plume migration at a specific, field scale site within a larger, regional scale aquifer, in the UK North Sea. The main objective of the study is to determine if the site is generally capable of storing the desired amount of CO_2 without causing an unsustainable increase in pressure or leading to migration of CO_2 over large distances. This preliminary site investigation will provide information on the feasibility of storing CO_2 at this site and the further data which will be needed to carry out a thorough site investigation. We also describe the methodology used to build a dynamic model for a site with little existing, direct data. The modelling choices made and the reasons behind them are given, providing a useful reference for building similar models in the future.

Geological Background

After the Carboniferous Variscan Orogeny, north – south extension and thermal subsidence in the North Sea during the Permian formed the Northern and Southern Permian Basins. They are separated by the Mid North Sea High. Rotliegend Sandstone was deposited into the Permian Basins and into the much smaller Moray Firth Basin. In the Late Permian, rifting in the Northern North Sea and rising sea levels led to the opening up of a seaway which allowed the Zechstein Marine Transgression to occur, forming the Permian Zechstein Salt (Taylor 1998). Subsequent east – west extension led to the formation of the Central and Viking Grabens which cross cut the Permian Basins.

Proposed storage site

The CCC prospect is located on the edge of the Northern Permian Basin within the Rotliegend and consists of three interconnected four-way dip closures which can be seen in the depth converted seismic data. It covers an area of 26.5 km^2 and is approximately 2600 m below sea level. The thickness of the storage formation at this point is uncertain as it is not possible to identify the base of the formation on the seismic data. Also, no wells penetrate the base of the Rotliegend in this area. It is estimated that beneath the CCC prospect the Rotliegend is 100 – 300 m thick.

The Rotliegend in our study area consists of Auk Formation deposits. The Auk Formation covers a large part of the Northern Permian Basin and is composed solely of sedimentary rocks. It was deposited at a time when the climate of the region was arid desert. Aeolian sandstones dominate the sequence with some fluvial and lacustrine facies also present. The prominent wind direction at the time was most likely from the north west (Glennie 1983; Glennie *et al.* 2003).

The Rotliegend forms a hydrocarbon reservoir in the nearby Auk field (Fig. 1(a)). Several studies have characterised the Rotliegend at the Auk field using core data (Heward 1991; Trewin *et al.* 2003). Heward (1991) divided the reservoir into several layers with different porosities and permeabilities according to the facies present within them. It is possible that this facies variation is also present in the CCC prospect.

Core data from wells near the storage site indicate that the lithology of the Rotliegend at the site is most likely similar to the fluvial and dune facies seen in the Auk field.

Caprock

The Zechstein Marine Transgression occurred during the late Permian and covered both the Northern and Southern Permian basins. Changes in sea level due to periodic glaciation and retreat led to several cycles of transgression and subsequent evaporation of the Zechstein Sea. This sequence of transgression and evaporation led to the deposition of a thick evaporite layer in the centre of the basin, predominantly composed of halite. A higher proportion of carbonates and anhydrite exists at the shallower edges of the basin. Some dolomitisation has occurred within the basin as a whole. Salt tectonics are common in the thicker, halite sections of the basin (Taylor 1998). This is when salt layers deform ductilely due the relatively low density salt being overlain by relatively high density strata. The movement of salt can disrupt the overlying strata potentially creating pathways for fluid leakage.

It is not possible to discriminate between the different Zechstein facies by interpretation of the seismic data. Dolomite rafts can have high porosity but it is thought, from seismic and well data, that there is > 800 m thickness of halite above the site which will provide a competent caprock with

sufficient sealing capacity. Salt tectonics can clearly be seen in the seismic data to the north east of the proposed storage site.

Base Unit

The Rotliegend in our study area is thought to lie unconformably upon Devonian Old Red Sandstone. This is not known for certain as no wells have penetrated the base of the Rotliegend in this area, however the Rotliegend is directly above Devonian strata in the Auk field (Trewin *et al.* 2003) and in the Argyll and Innes fields to the east of the storage site (Heward *et al.* 2003). Alternatively the Rotliegend of the storage site could lie on top of Carboniferous strata. However, it is possible that both the Devonian Old Red Sandstone and Carboniferous rocks in the area have similar porosity and permeability characteristics to the Rotliegend Sandstone.

Modelling

The model has been built to satisfy in part the requirements of the EU Directive (European Union 2009), for characterisation of the dynamic behaviour of injected CO_2 in a potential storage site. At present the available input data is not sufficient to provide a complete site characterisation which assesses all aspects required by the EU Directive. The main parameters investigated using this model are the storage capacity of the intended trap, pressure buildup within the storage site and the migration of the CO_2 plume.

A choice of modelling methods for site characterisation is available. The simplest of these are analytical methods which provide analytical solutions for one or two model variables such as storage capacity (Zhou *et al.*, 2008), pressure buildup with CO_2 injection (Mathias *et al.*, 2008; Zhou *et al.* 2008; Mathias *et al.* 2011), or the radius of the CO_2 plume (Nordbotten *et al.* 2005). These methods are useful as they provide a quick assessment of certain characteristics of a site. However, they require some simplifying assumptions to be made. A common limitation of analytical models is that they are unable to account for heterogeneity in either formation properties or model geometry. As we have access to stratigraphic relief data, in the form of an interpreted seismic layer, we can better model storage capacity, CO_2 migration and pressure buildup specific to our site using a 3D numerical model which incorporates the geometry data.

3D numerical modelling can be undertaken using several different methods. One potential option is to use streamline based models (Obi and Blunt 2006; Qi *et al.* 2009). Here the model domain is split into small grid blocks and a finite difference approximation is used to calculate pressure in each grid block. The pressure field is then used to trace streamlines which show the fluid flow paths within the model. Flow equations are solved in one dimension, along the streamline, for several timesteps to show the migration of different phase saturations within the storage site. After a certain global timestep size the average saturation of each grid block is calculated from the saturation of the streamlines running through it, the pressure field is updated and the locations of the streamlines are retraced. The whole process is then repeated. This method is computationally efficient as the flow equations are only solved in one dimension, along the streamlines. Also, fewer time consuming pressure calculations have to be carried out. However, streamline simulation is only suitable for modelling systems where the pressure, and therefore the location of the streamlines, does not change much during the relatively large pressure timesteps. As our model involves CO_2 injection with no accompanying production, the pressure change in the system is quite large. Consequently, streamline simulations may not be suitable in this context.

Another possible option is to use a vertical equilibrium model (Gasda *et al.* 2009; Gasda *et al.* 2011; Nilsen *et al.* 2011). In this method the model domain is discretised in the horizontal direction but only contains one layer in the vertical direction. The fluids in each cell are assumed to be in a gravitationally stable configuration (vertical equilibrium), therefore no flow in the vertical direction is modelled. Horizontal flow in the model is solved-for using Darcy's law. The height of the interface between fluid phases (CO_2, CO_2 saturated brine, brine) in each cell can then be found, using an analytical solution based on the phase saturations. This method is more computationally efficient than a full three dimensional model as the flow equations are only solved in two dimensions. It allows the horizontal plume spread and the segregation between the different fluid phases to be modelled. However, the assumption that the storage site is in vertical equilibrium means that it is not possible to account for heterogeneity and anisotropy in the vertical direction. Consequently, a vertical equilibrium model is unsuitable for assessing effects associated with layering within formations, such as those potentially present within the Rotliegend.

In this study, we consider a more conventional 3D, regular, grid based model which uses an integrated finite difference method to solve the flow and transport equations (Narasimhan & Witherspoon 1976). This is more computationally expensive than other methods as it requires the model to be discretised into a three dimensional grid and therefore the equations have to be solved for more gridblocks at each timestep. However, the chosen method will enable us to better model the pressure increase during the injection period and to include vertical anisotropy in the form of anisotropic permeability and layering within the model.

Specifically, modelling has been performed using TOUGH2-MP (Zhang *et al.* 2008), the parallel version of the TOUGH2 numerical code for modelling multiphase flow in porous media (Pruess *et al.* 1999). It has been used in conjunction with the ECO2N equation of state module (Pruess 2005), which models mixtures of H_2O-CO_2-NaCl and has been designed specifically to represent conditions applicable to CO_2 storage in saline aquifers. Code comparison studies (Pruess *et al.* 2004) have shown TOUGH2 to be a robust code, capable of modelling complex systems relating to geological storage of CO_2. It is widely used for CO_2 storage simulations (e.g. Chadwick *et al.* 2009a; Doughty 2010; Chasset *et al.* 2011).

The model covers an area of about 15.75 km by 14.25 km. This encompasses the CCC Prospect but does not extend to the stratigraphic pinchout of the Rotliegend which could form a secondary trap in the event of CO_2 escaping laterally from the CCC Prospect. In the interest of reducing the computational cost of modelling it was decided at this early stage to only model the CCC Prospect and the area immediately surrounding it.

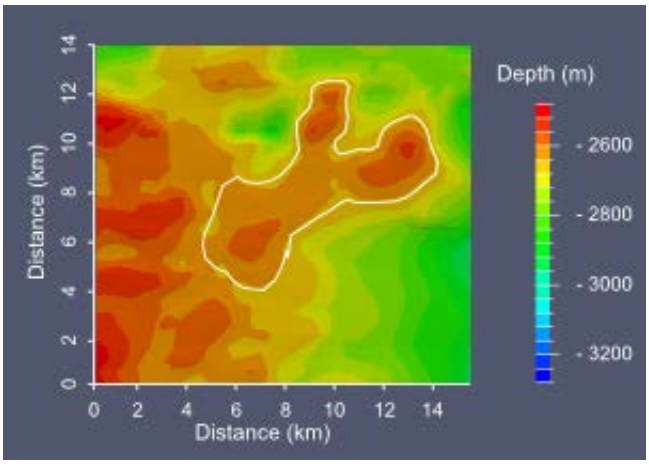

Fig. 2. *Depth map of top of the model. White line indicates outline of CCC Prospect.*

The model is rectangular in area. The base of the Rotliegend layer cannot be distingushed in the seismic data. A formation thickness of 320 m has been chosen for the base case model. The relief of the top surface of the model has been interpolated from the depth converted seismic surface of the top of the Rotliegend (Fig. 2). As the base of the Rotliegend cannot be seen in the seismic data, the base of the model has been given the same relief as the top of the model.

The available seismic data is old and was interpreted using only sparse coverage of well data picks. This is often the case for CCS modelling studies of previously unused sites (e.g. Noy *et al.* 2012; Schäfer et al. 2012). Seismic data must be integrated with well data to provide a reasonable estimate of reservoir depth and the thickness of layers within the reservoir. Large uncertainties can be introduced into the data when well data is sparse and well locations are far from the storage site. To address this issue we have varied reservoir thickness in one of the model runs. Other dynamic modelling studies of storage sites within saline formations have used models with flat top and bottom surfaces (Hovorka *et al.* 2004; Chasset *et al.* 2011). This is due either to a lack of significant undulation in the surfaces of the modelled units or a lack of seismic data over the modelled site. To assess the impact of using a model with flat surfaces we have run some simulations with flat top and bottom surfaces.

The horizontal resolution of the model is 5 m around the injection well increasing to 500m at the edges of the model. To accurately model injection well pressure a very fine horizontal grid resolution (~ 5 mm) is needed around the injection well (Mathias *et al.* 2011). As the purpose of our model is to look at the overall capacity of the storage site to store injected CO_2 it was not deemed necessary at this stage to carry out detailed modelling of injection pressures. Therefore, a larger grid resolution near the well bore has been chosen in order to increase the computational efficiency of simulations. This approach of having a relatively large injection cell is taken by several studies investigating field scale effects of CO_2 injection, particularly for models using fully 3D rectangular grids (Doughty 2010; Noy *et al.* 2012). Yamamoto *et al.* (2009) used a Voronoi mesh which allowed them to have very fine grid resolution around their modelled injection wells. However, in their study it was important to model the effects of several closely spaced injection wells and the corresponding brine migration caused by the pressure increase around the wells. This is not the case in our work.

Vertical resolution is 1 m for the first 10 m below the caprock. Beneath the top 10 m of the model the vertical resolution is 10 m. Yamamoto & Doughty (2011) showed that a coarse vertical grid resolution reduced the maximum radial plume extent at the top of their model, particularly when the injection rate was low (0.1 Mt/a). The injection rate in our models is much higher than this. However, the grid resolution has been increased at the top of the model in order to better capture the plume spread at the top of the storage site.

The total number of gridblocks in the base case model is 350714 (94 x 91 x 41).

Initial and boundary conditions

The initial conditions used in the models have been informed by well data and literature data. Where possible, direct data from the Rotliegend formation close to the CCC Prospect have been used. Literature observations regarding nearby analogues and rocks with similar lithologies have been used in preference to more general observations. Empirical observations from the literature have been given priority over theoretical relationships.

Pressure information is available from a pressure study undertaken at the site using nearby well data and published information. The site is thought to be slightly overpressured compared to the hydrostatic pressure gradient. Pressure at the top of the site is ~ 33 MPa. The fracture pressure of the Zechstein caprock is estimated to be 47 MPa. In our models pressure has been set at 33 MPa at a depth of 2600 m and a hydrostatic gradient has been allowed to equilibrate.

A temperature of approximately 90°C, taken from nearby well logs, has been chosen as the formation temperature at 2600 m depth. A geothermal gradient of 30 °C/km has then been applied to the model. This is a reasonable value for the geothermal gradient in the area of the storage site (Cornford 1990).

No direct data is available about existing fluids within the formation. We have assumed that the storage site is initially filled with brine. A salinity of 10.5 % has been used similar to the salinity of formation fluids in the Auk field (Trewin *et al.* 2003). The effect of salt precipitation due to formation dry-out near the injection well (Kim *et al.* 2012) has not been looked at. This effect has implications for injection pressures but has not been included as we are not carrying out detailed modelling of formation injectivity.

Appropriate boundary conditions are required to model pressure buildup and fluid migration accurately. The thickness of the salt (up to 1 km) and its low permeability mean it is unlikely that CO_2 will leak into the caprock, unless the fracture pressure is exceeded. Therefore a no flow boundary condition has been implemented at the top of the model. The assumption of a no flow boundary at the top seal of the model is frequently used to represent the boundary between a relatively high permeability formation and an extensive, low permeability caprock (Doughty 2007; Hazignatiou *et al.* 2011). Noy *et al.* (2012) show that reducing the permeability of the caprock leads to an increase in the pressure footprint of the plume. Using a no flow boundary condition instead of modelling the caprock essentially reduces the permeability of the caprock to zero, thus allowing a conservative pressure estimate to be made. The advantage of not modelling the caprock explicitly is a reduction in model complexity and associated computation time.

The pressure study of the site suggests that the storage formation is not compartmentalised. To reflect this, an open boundary condition (constant pressure) has been imposed at the lateral edges of the model. The nature of the unit beneath the storage site is unknown although it is suspected to be Devonian Sandstone, similar in nature to the Rotliegend Sandstone. If this is the case, the bottom boundary will probably allow flow across it and should therefore be modelled as an open boundary. Sensitivities have been run with closed base boundaries to look at the extreme case of a very low permeability unit underlying the storage site.

Input parameters

Values for input parameters used for modelling are shown in Table 1.

	Base case	**Ranges modelled**
Pressure	33 MPa	-
Temperature	90°C	-
Salinity	10.5 %	-
Porosity	0.19	0.10 – 0.27
Permeability	28 mD (2.76E-14 m^2)	21 – 33 mD (2.07E-14 m^2 – 3.26E-14 m^2)
kv/kh	0.1	-
Pore compressibility	1.05E-09 Pa^{-1}*	8.73E-10 Pa^{-1} – 1.05E-09 Pa^{-1}
Relative permeability	Function to fit Viking 2 data†	-
Capillary pressure	Function to fit Viking 2 data†	-
Isothermal	Yes	-
Diffusion	No	-
Reservoir thickness	320 m	120 m – 320 m
Injection interval	40 m	40 m – 70 m
Injection rate	2.5 Mt a^{-1}	-
Simulation length	20 yrs	Post injection – 100 yrs

Table 1. *Model input parameters. * From Jalalh (2006). † From Bennion and Bachu (2006)*

Porosity and permeability data can either be measured directly from cores or be calculated from borehole data. There are various ways of calculating porosity and permeability depending on the data available. Several authors have used depth / porosity correlations and then porosity / permeability correlations of surrounding units to calculate porosity and permeability of the modelled units, based on their depth (Eigestad *et al.* 2009; Hazignatiou *et al.* 2011). This has allowed them to calculate porosity and permeability for areas where no direct porosity and permeability measurements are available.

In our case, porosity values for the Rotliegend are representative values taken from sonic logs of nearby wells and the literature, and are in the range 10 – 27 % with the most likely value being ~19 % (Selley 1978). Porosity values from the sonic logs were calculated using the equation given by

312 Wyllie et al. (1958). No correction was made for clay content as the part of the Rotliegend
313 penetrated by the logs consists of relatively clean quartz arenite.

314 Horizontal permeability values (k_h) have been taken from core flood data of Rotliegend samples
315 from nearby wells. Permeabilities range from 21 mD (2.07E-14 m^2) for the finely laminated facies, to
316 33 mD (3.26E-14 m^2) for the massive sand facies, with 28 mD (2.76E-14 m^2) for the diffuse laminated
317 facies, taken as the most likely case. The ratio of vertical to horizontal permeability (k_v/k_h) has been
318 chosen as 0.1. A k_v/k_h of 0.1 is similar to values chosen in several studies to represent the fact that
319 permeabilities in siliciclastic rocks are generally greater parallel to the bedding planes (e.g. Ghomian
320 *et al.* 2008; Doughty 2010). The presence of clays within the reservoir would reduce this
321 permeability ratio (Ringrose et al. (2005)) however core data indicates that clay content within the
322 Rotliegend near the CCC Prospect is negligible. Pore compressibility has been estimated using a
323 correlation by (Jalalh 2006) which was calculated in the laboratory and relates porosity and pore
324 compressibility in sandstones.

325 Relative permeability and capillary pressure data have come from the laboratory studies on the
326 Viking 2 sandstone by (Bennion & Bachu 2006). Viking 2 sandstone was chosen as it has similar
327 porosity and permeability values to the estimated values for Rotliegend at our site. The effect of
328 hysteresis, where the multiphase flow properties of the pore space are history dependent, has not
329 been included in our model. Including hysteresis would lead to an increase in residually trapped CO_2
330 and a reduction in the amount of mobile CO_2 which is able to move through the formation (Doughty
331 2007). Consequently CO_2 mobility in our models is at its upper limit, providing a maximum estimate
332 of plume spread.

333 Temperature change through time and dissolution of CO_2 into the brine have not been modelled.
334 Modelling temperature changes can be important when considering the effect of Joule-Thomson
335 cooling (Oldenburg 2007; Mathias *et al.* 2010). This is where CO_2 cools as it undergoes rapid
336 expansion due to a large drop in pressure. This could be the case for injection into a depleted oil or
337 gas reservoir which is at a low pressure but is unlikely to be as important for injection into an aquifer
338 at a pressure similar to that of the injected supercritical CO_2. Dissolution of CO_2 into the resident
339 brine is an important trapping mechanism. However, in the interest of computational efficiency we
340 have chosen not to model dissolution as the effect of dissolution is relatively small during the early
341 stages of CO_2 injection. Prior to the onset of convection, CO_2 can only dissolve in residually trapped
342 brine which is in contact with free-phase CO_2. The amount of CO_2 which can dissolve is controlled by
343 the solubility limit of CO_2 in the brine. CO_2 solubility limit in brine, which is dependent on pressure
344 and temperature conditions, can be calculated using the equation of state provided by Spycher and
345 Pruess (2005). Assuming a residual brine saturation of 0.423 (i.e., the Viking 2 core) at 33 MPa and
346 90°C, the amount of CO_2 expected to dissolve in residually trapped brine would represent around
347 3.7% of the total mass of injected CO_2.

348 The model injection point is located just off crest of the largest dome in the CCC structure. For
349 operational purposes it would be best to inject CO_2 down dip from the structure to be filled.
350 Buoyancy would then transport the CO_2 to the desired location, allowing more of the reservoir to be
351 swept by the CO_2 and therefore increasing residual trapping. In our preliminary model it was
352 decided to locate the injection point much closer to the top of the structure in order to demonstrate

containment within the CCC Prospect. This ensures that all the modelled migration of CO_2 is within the CCC Prospect, at least at the beginning of the simulation.

Injection has been carried out from a vertical well at a rate of approximately 2.5 Mt a^{-1} for 20 years. The completion interval varies from 40 m to 70 m. This interval is purposefully small to allow a more conservative estimate to be made of pressure and CO_2 saturation around the injection point. Post injection modelling for most models has been carried out for up to 100 years. Convergence issues, particularly with the layered models meant this was not possible for all models.

Input parameters for most of the models are uniform throughout the model domain. Some heterogeneous models were run, where differing permeability and porosity values were assigned to layers within the model. However, no allowance was made in any of the models for lateral heterogeneity in the storage site. This is due to a lack of data describing lateral heterogeneity within the site.

Results

Base Case

367

Model	s01a	s01a5	s01b	s01b4	s01c	s01c2	s01d	s01e	s01f	s02a	s02a2	s02a3	s02a4	s03a	s04f	s07a
Permeability Minimum – Min Most likely – ML Maximum – Max	ML	ML	Min	Min	Max	Max	ML	ML	ML	ML	ML	Min	Max	ML	ML	ML
Porosity Minimum – Min Most likely – ML Maximum – Max	ML	Max	Min	ML	Max	ML	ML	ML	ML	ML	ML	ML	ML	ML	ML	ML
Thickness 320 m 120 m	320 m	320 m	320 m	320 m	320 m	320 m	320 m	320 m	320 m	320 m	320 m	320 m	320 m	320 m	120 m	320 m
Layers No Yes	No	No	No	No	No	No	No	No	No	Yes	Yes	Yes	Yes	No	No	Yes
Base Boundary Open Closed	Open	Open	Open	Open	Open	Open	Closed	Open	Closed	Closed	Open	Open	Open	Open	Closed	Open
Lateral boundaries Open Closed	Open	Open	Open	Open	Open	Open	Open	Closed	Closed	Closed	Open	Open	Open	Open	Closed	Open
Topography Yes No	Yes	Yes	Yes	Yes	Yes	Yes	Yes	Yes	Yes	Yes	Yes	Yes	Yes	No	Yes	No
Max. Pressure Increase* 20 yrs (MPa)	1.50	1.52	1.62	1.68	1.36	1.36	2.92	1.50	5.34	3.76	0.68	1.97	0.58	1.49	13.53	0.64
Max. Pressure Increase* 120 yrs (MPa)	0.25	-	0.29	0.26	0.23	-	0.26	0.25	3.17	-	-	-	-	0.19	7.76	-
Plume diameter‡ 20 yrs (km)	1740	1195	2345	1351	1345	1842	1934	1740	1745	1351	2145	0	2872	1740	2682	1448
Plume diameter‡ 120 yrs (km)	3266	-	4559	2872	2782	-	3392	3266	3198	-	-	-	-	3393	3571	-

368

369

Table 2. *Summary of model configurations and results. *Pressure measured at top of reservoir along cross section line. † Plume diameter measured at top of reservoir along cross section line*

Table 2 shows the configuration of all models run and a summary of the results.

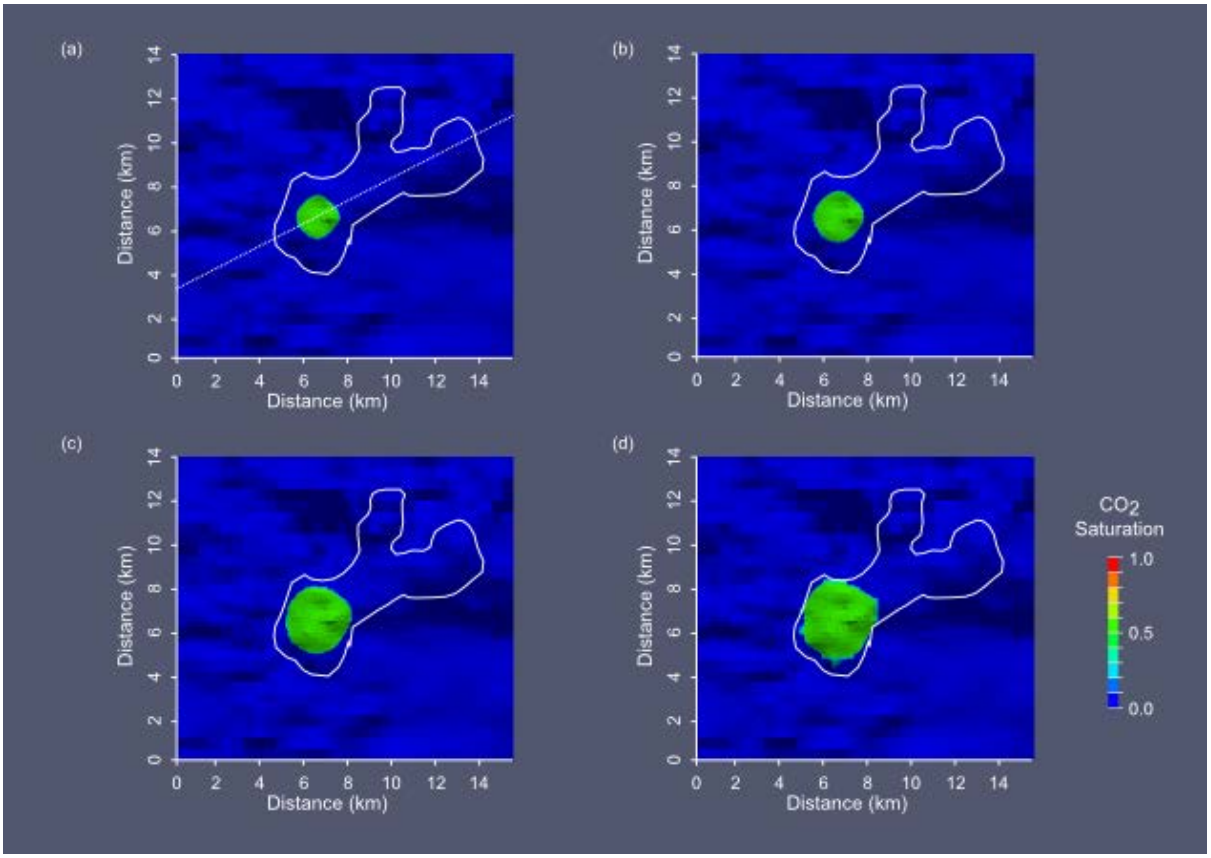

Fig. 3. *s01a – CO_2 saturation at the top of the storage site, (**a**) 20 years, (**b**) 30 years, (**c**) 70 years, (**d**) 120 years. Shading indicates surface topography. White line indicates outline of CCC Prospect. White dashed line indicates location of cross-section in Figs. 4, 11, 12, 13.*

Fig. 3 shows the extent of the CO_2 plume, beneath the top of the storage site, through time for the base case scenario (See Table 2, (s01a) - 320 m thick, open lateral and base boundaries, most likely porosity and permeability values). The white line indicates the outline of the CCC Prospect at spill point taken from the depth converted seismic. All the CO_2 is contained within the structure up to 100 years after the end of injection. However, the CO_2 plume is close to the edge of the structure at the end of the simulation and in time may migrate out of it.

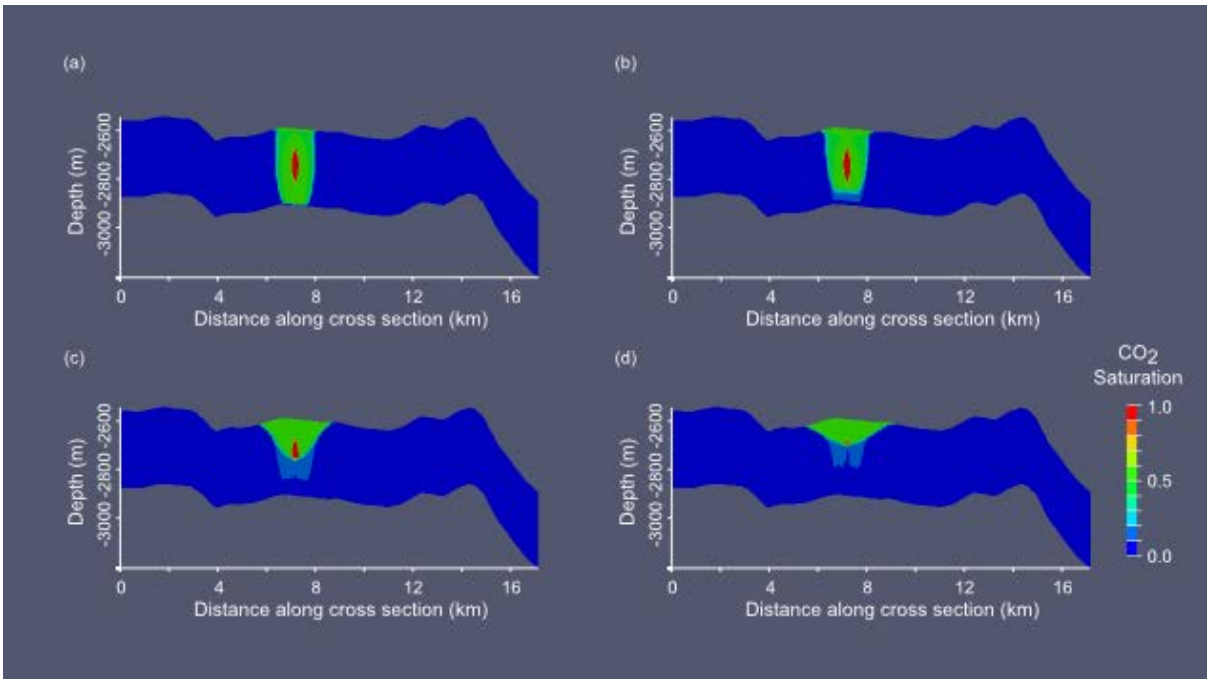

384

385 ***Fig. 4.*** *s01a - CO_2 saturation for a cross section through the storage site, (**a**) 20 years, (**b**) 30 years, (**c**)*
386 *70 years, (**d**) 120 years. 10 x vertical exaggeration. Cross section location shown in Fig. 3.*

387 A cross section through the plume (Fig. 4) shows that CO_2 concentration is highest around the
388 injection point. At the end of 20 years of injection CO_2 fills the whole thickness of the storage site.
389 After injection finishes the plume migrates upwards under buoyancy and spreads laterally beneath
390 the caprock. The CO_2 does not appear to have stabilised by this time, which would be indicated by
391 the base of the CO_2 saturated part of the reservroi being level. It is most likely that the CO_2 will
392 migrate into the dip closure to the right of the injection point (at ~ 14 km along the cross section)
393 following the path with the highest stratigraphic relief.

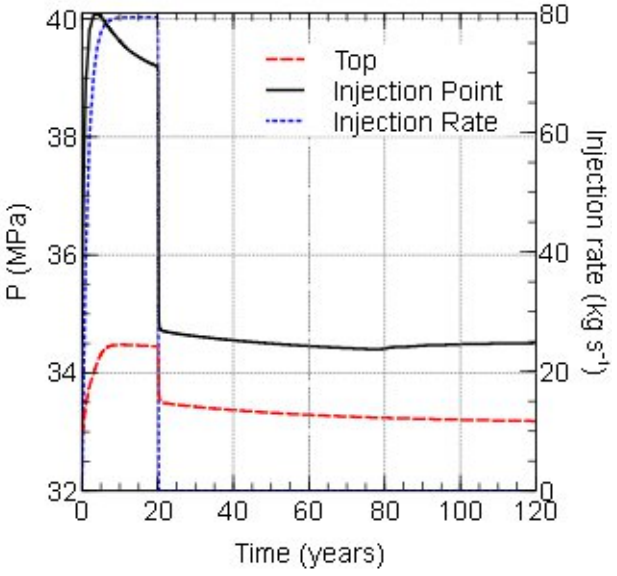

394

Fig. 5. *s01a (see Table 2)- Pressure (P) through time for location immediately to the east of the injection point and at the top of the storage site above the injection point. Injection rate is also shown.*

Fig. 5 shows the pressure through time next to the injection point and at the top of the storage site, directly above the injection point. Injection rate is also shown. At both locations the pressure increases as the cumulative amount of injected CO_2 increases. Near the injection point pressure peaks at 40.1 MPa after 4 years and then decreases. At the top of the storage site pressure increases more slowly and reaches a peak of 35.5 MPa at around 10 years. Pressure in all locations never exceeds the caprock fracture pressure of 47 MPa.

The initial pressure peak during the injection period is probably related to modelling effects associated with a rapid increase in pressure when the injection begins (see Mathias *et al.* 2011). It can be reduced by further shaping of the injection rate or a reduction in grid resolution around the injection point. Detailed modelling of injection has not been attempted in this study therefore maximum pressures for subsequent models have been taken at the end of the injection period where this effect is reduced.

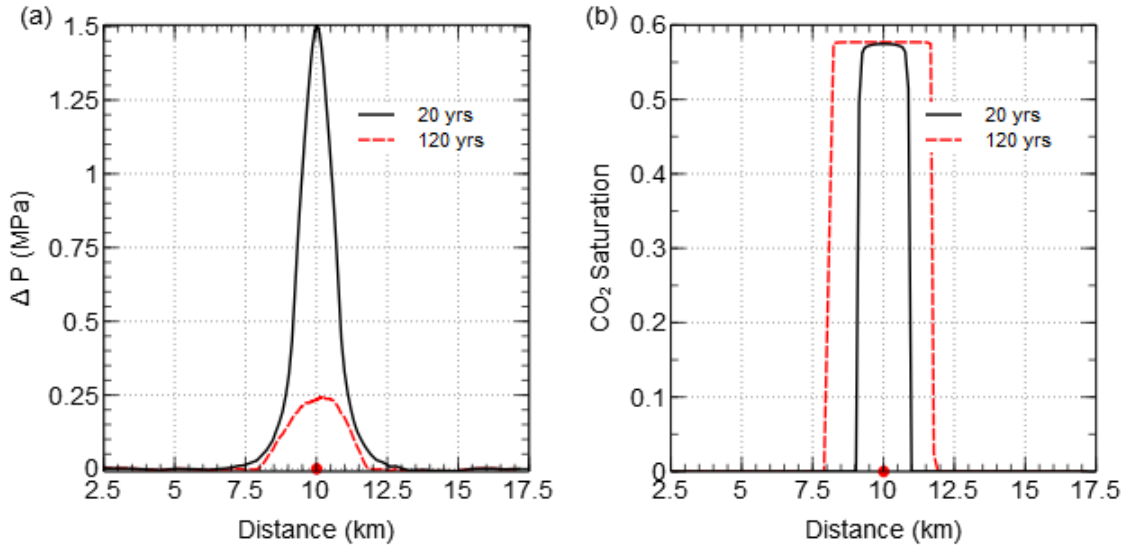

Fig. 6. *s01a (see Table 2) - (**a**) Pressure buildup (Δ P) and (**b**) CO_2 saturation, along cross section at the top of the storage site. Injection point indicated by the red circle. Cross section location shown in Fig. 3.*

The pressure increase at the top of the storage site, along the line of the cross section, can be seen in Fig. 6(a). At the end of injection (20 years) the highest pressure increase is 1.50 MPa above virgin pressure, located above the injection point. Fig. 6(b) shows the extent of the CO_2 plume at the top of the storage site. It can be seen that the pressure increase extends approximately 3 km on either side of the CO_2 plume. In the rest of the model pressure has returned to its starting value. After 120 years the pressure increase is 0.28 MPa. The highest pressure increase corresponds to the location of a structural stratigraphic high in the model where the CO_2 column beneath the caprock is thickest.

The pressure increase does not extend further than the edge of the CO_2 plume at the end of the simulation.

Sensitivities

Boundary conditions

As the boundary conditions of the sides and the base of the model are not well constrained, several models have been run to test the sensitivity of results to a change in boundary conditions.

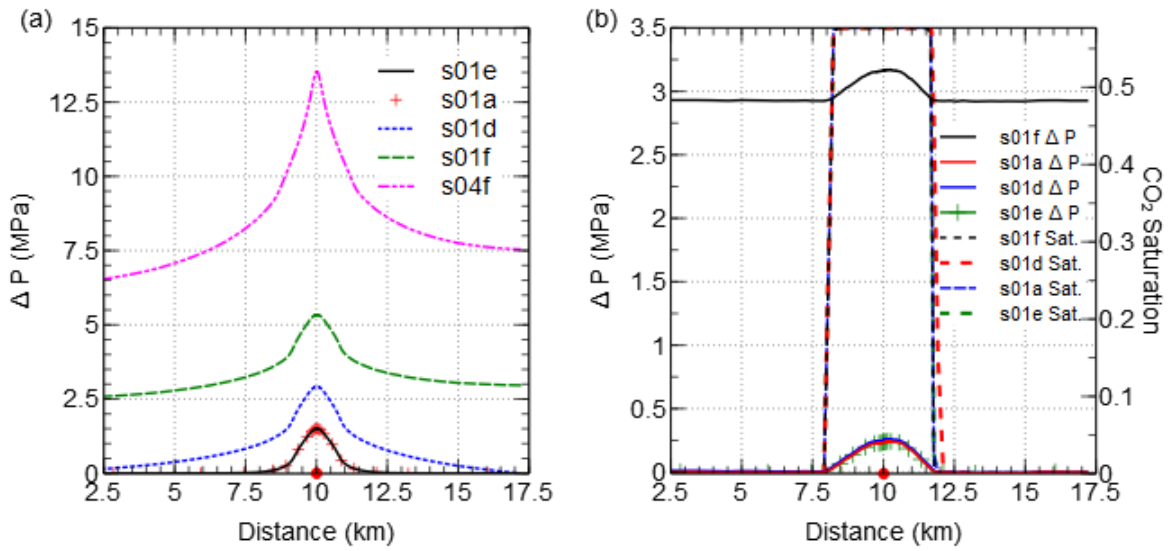

Fig. 7. *(**a**) Pressure buildup (Δ P) along cross section at the top of the storage site for models with different boundary conditions at 20 years. Injection point indicated by the red circle. (**b**) Pressure buildup and CO_2 saturation (Sat.) along cross section at the top of the storage site, for models with different boundary conditions, at 120 years. s01a – open base, open sides, s01d – closed base, open sides, s01e – open base, closed sides, s01f – closed base, closed sides, s04f – closed base, closed sides, thin storage site (see Table 2). Injection point indicated by the red circle. Cross section location shown in Fig. 3.*

The pressure buildup at the end of injection is smallest for models with open (constant pressure) base boundaries (Fig. 7(a)). For the two models run with open base boundaries the pressure increase is almost identical at 20 years, regardless of the nature of the lateral boundaries. Having closed boundaries on all sides of the model leads to a higher pressure buildup with a maximum pressure increase of 5.34 MPa above the injection point.

The thickness of the storage site is unknown. Therefore a worst case scenario model was developed with a relatively thin storage site (120 m) and closed boundaries on all sides. Pressure buildup in this model is much higher than in other models (Fig. 7(a)). The pressure reaches a value of 46.5 MPa at the end of injection, which is very close to the estimated caprock fracture pressure of 47 MPa. The peak in pressure is located above the injection point.

After 120 years the pressure has returned to starting pressure everywhere except beneath the CO_2 plume, for models with at least one open boundary (Fig. 7(b)). The pressure profile is the same for all

models but pressures in the model with closed side and base boundaries are approximately 2.9 MPa higher than pressures in the other models. The plume diameter at 120 years is very similar in all models.

Permeability / Porosity

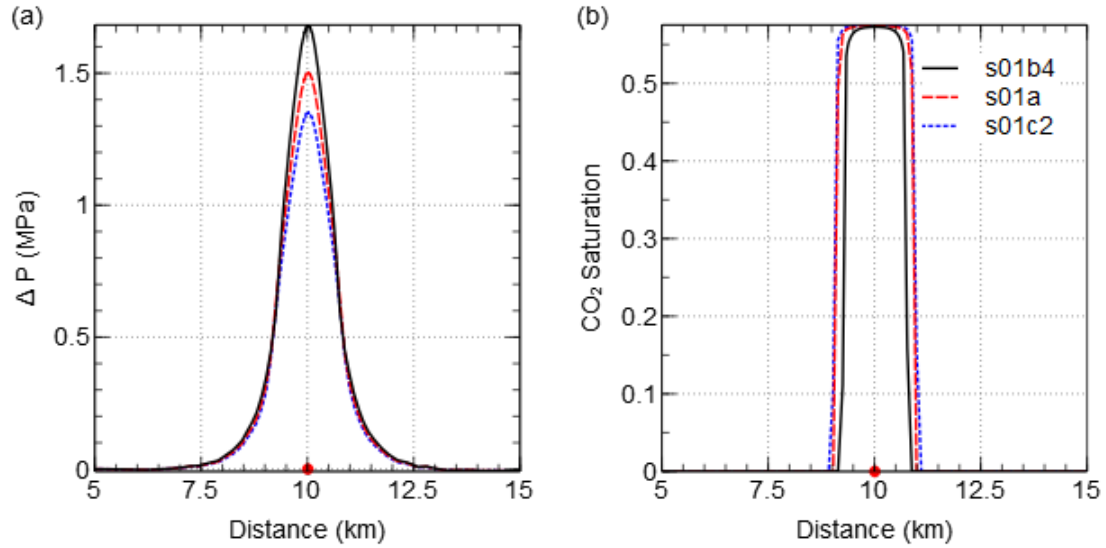

Fig. 8. *(**a**) Pressure buildup (Δ P) and (**b**) CO_2 saturation, along cross section at the top of the storage site, for models with different permeability, at 20 years. s01a – Most likely permeability, s01b4 – Min. permeability, s01c2 – Max. permeability (see Table 2). Injection point indicated by the red circle. Cross section location shown in Fig. 3.*

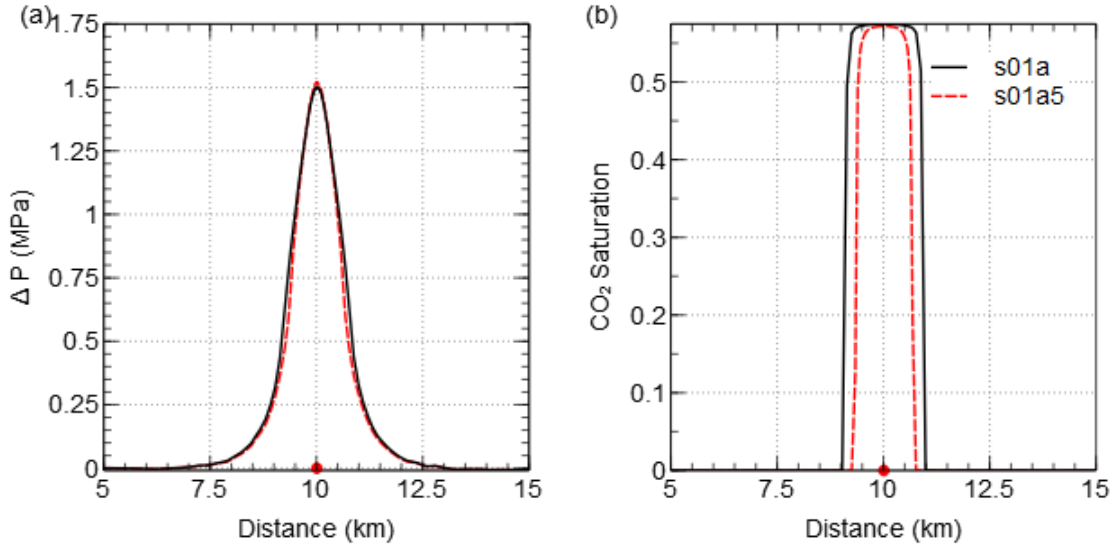

458 ***Fig. 9.*** *(**a**) Pressure buildup (Δ P) and (**b**) CO_2 saturation, along cross section at the top of the storage*
459 *site, for models with different porosity, at 20 years. s01a – Most likely porosity, s01a5 – Max.*
460 *porosity. Location of injection point indicated by the red circle. Cross section location shown in Fig. 3.*

461

462 Models were run with minimum and maximum permeability and porosity values in addition to the
463 most likely values used in the base case. Lowering the permeability results in an increase in pressure
464 buildup and a decrease in plume diameters after 20 years (Fig. 8). Increasing porosity values leads to
465 a small increase in maximum pressure buildup. Having a higher porosity reduces the plume diameter
466 at the top of the model after 20 years (Fig. 9).

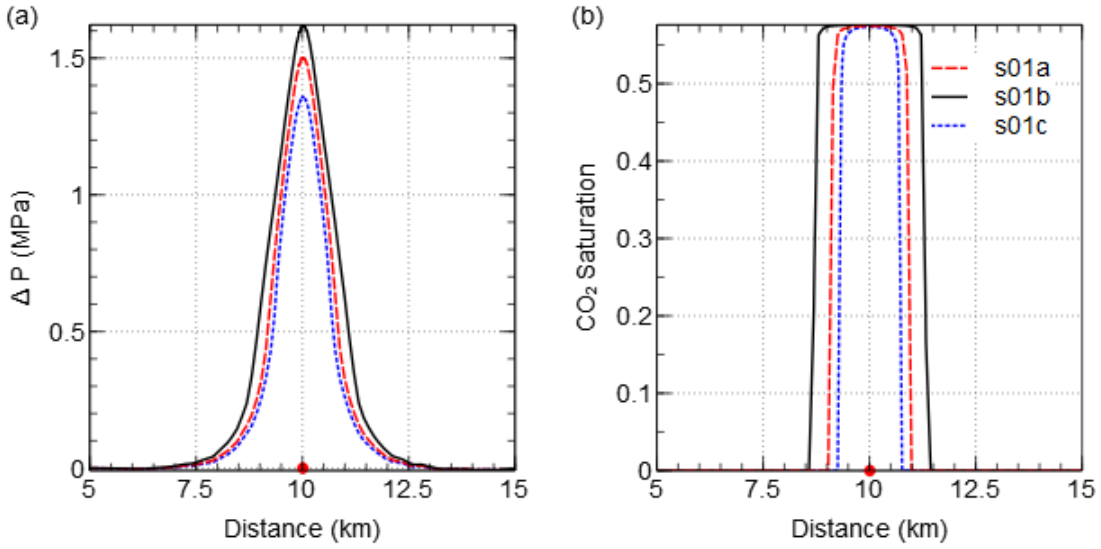

467

468 **Fig. 10.** (**a**) Pressure buildup (Δ P) and (**b**) CO_2 saturation, along cross section at the top of the
469 storage site, for models with varying porosity and permeability, at 20 years. s01a – Most likely
470 porosity / permeability, s01b4 – Min. porosity / permeability, s01c2 – Max. porosity / permeability
471 (see Table 2). Location of injection point indicated by the red circle. Cross section location shown in
472 Fig. 3.

473

474 The pressure buildup and plume diameters which occur when both the porosity and permeability
475 are changed at the same time show an increase in pressure buildup and plume diameter when the
476 permeability and porosity are lower (Fig. 10).

477 ***Layering***
478

Facies	Thickness of layer (%)	Porosity (%)			Permeability (mD)		
		Min	Max	Mean	Min	Max	Mean
1. Fluvial	35	9	19	14	1	100	50.5
2. Aeolian	35	12	25	22	80	1000	540

3. Interdune	25	5	19	15	0.8	10	5.4
4. D facies	5	2	10	6	0.1	1	0.55

Table 3. *Layer thicknesses and properties*

Internal facies variation has been observed in Rotliegend reservoirs in the Auk and Argyll fields (Heward 1991; Heward *et al.* 2003). These variations have distinct permeability and porosity values which will affect fluid flow in the reservoir. A general layering scheme consisting of four layers has been derived from these papers, to represent possible layering in the Rotliegend at the location under investigation (Table 3). The thicknesses of layers have been defined as percentages to account for uncertainties in the total Rotliegend thickness.

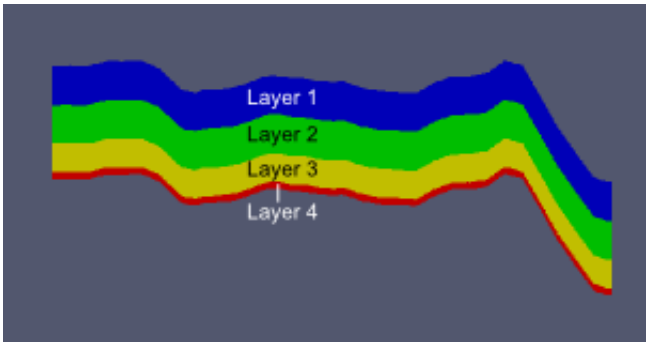

Fig. 11. *Slice through model showing layering. Numbers correspond to layers in Table 3. Red circle indicates location of injection point. 10 x vertical exaggeration. Cross section location shown in Fig. 1.*

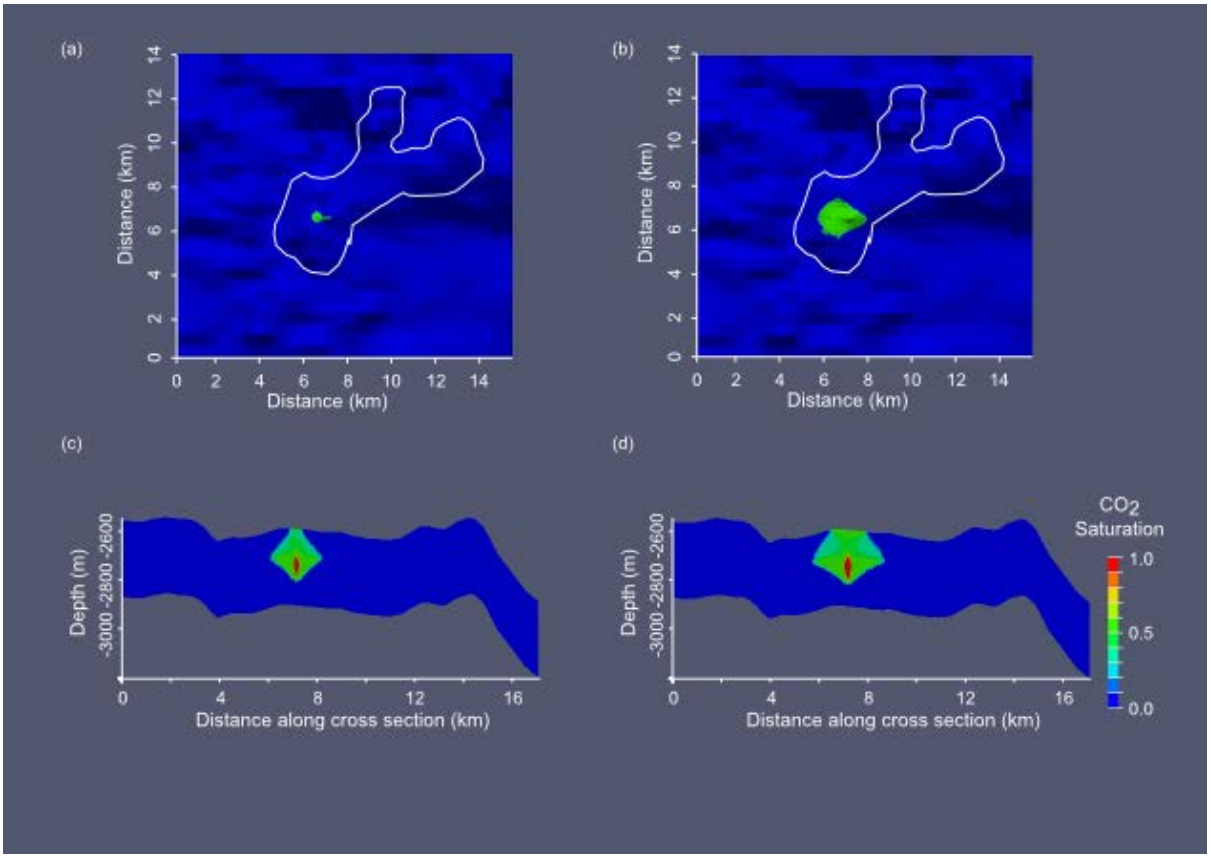

Fig. 12 *s02a2 – CO_2 saturation at the top of the storage site, for the layered storage site model, (**a**) 10 years, (**b**) 20 yrs. White dots indicate outline of CCC prospect. CO_2 saturation for a cross section*

*through the layered storage site model (**c**) 10 years, (**d**) 20 yrs. 10 x vertical exaggeration. Cross section location shown in Fig. 3.*

Fig. 11 shows a cross section of the layered model. The presence of layers in the model modifies the shape of the CO_2 plume as it rises towards the top of the storage site. The CO_2 spreads laterally beneath the boundary between layers 1 and 2 (Fig. 12 (c) & (d)). This reduces the amount of CO_2 reaching the top of the storage site compared to the homogeneous model and therefore reduces the plume diameter at the top of the model (Fig. 12 (a) & (b)). It can also be seen in Fig. 12 that the CO_2 plume footprint is more irregular in shape than in other models. The plume spreads further to the east of the injection point, following an area of high relief.

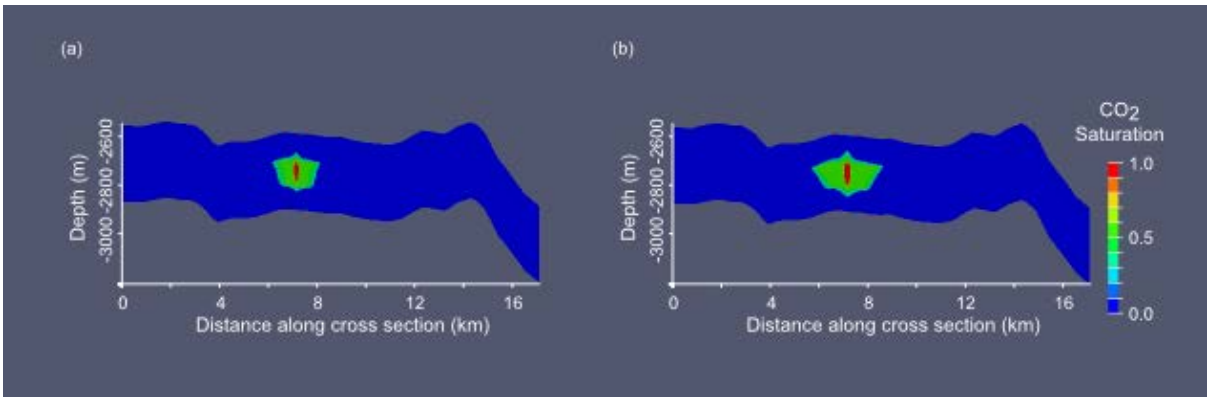

***Fig. 13.** s02a3 - CO_2 saturation for a cross section through the layered storage site model, with low permeability, (**a**) 10 years and (**b**) 20 yrs. 10 x vertical exaggeration. Cross section location shown in Fig. 3.*

Permeability in the layered model has a large effect on the plume footprint and the pressure buildup. When the permeability is higher the plume footprint is much larger than in the model with average permeability. In the low permeability model the CO_2 does not reach the top of the model after 20 years of injection. Nearly all the CO_2 is still contained within layer 2 (Fig. 13). The layers reduce pressure buildup because they compartmentalise free CO2; the exception being in the case of the low permeability layered model, where the maximum pressure increase after 20 years injection is nearly 2 MPa.

Stratigraphic relief

To assess the impact of irregular stratigraphic relief on results, two additional models were built with flat, uniform surfaces, one with layers and one without.

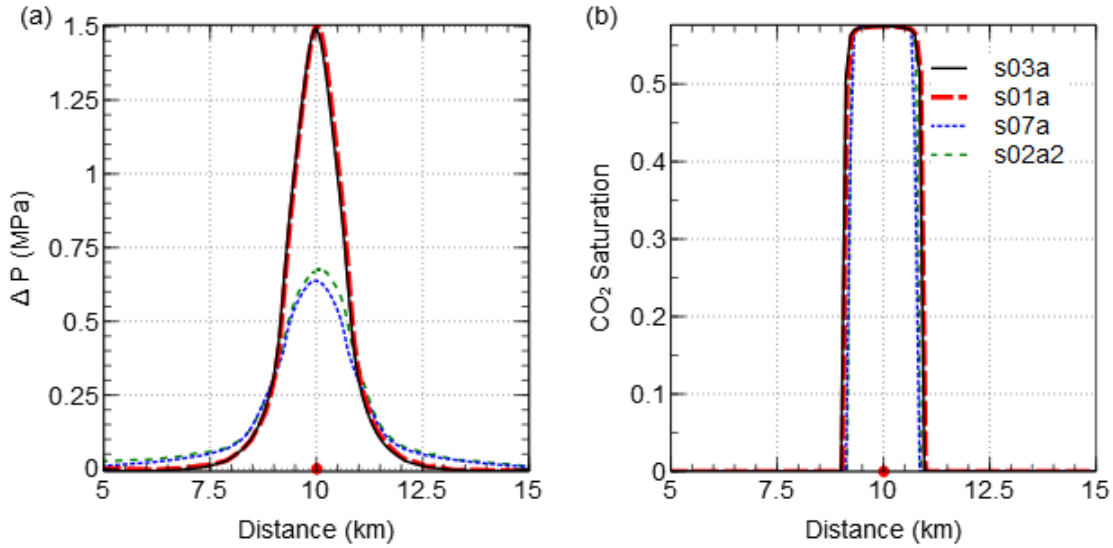

Fig. 14. *(**a**) Pressure buildup (Δ P) and (**b**) CO_2 saturation, along cross section at the top of the storage site, for flat and layered models, at 20 years. s03a – Flat, no layers, s01a – Irregular topography, no layers, s07a – Flat, layers, s02a2 – Irregular topography, layers (see Table 2). Location of injection point indicated by the red circle. Cross section location shown in Fig. 3.*

Comparison of the non-layered models, both with and without irregular surfaces, shows that the effect of irregular stratigraphy on pressure buildup and plume spread is small (Fig. 14).

By contrast, in the layered models irregular stratigraphy has a noticeable effect on the pressure buildup and plume spread. In the flat, layered model the plume footprint and corresponding pressure buildup is symmetrical around the injection point. In the layered model with irregular stratigraphy the higher pressure buildup is observed in the region to the east of the injection point related to the irregular plume footprint shown in Fig. 12.

Discussion

Pressure Buildup and Plume Diameter

The largest pressure increases are observed in the models with closed boundaries on all sides. This is because the pressure buildup in the storage site is unable to dissipate (see Mathias *et al.* 2011). However, only in the thin, closed boundary model (s04f) is the pressure close to fracture pressure. Similar results have been found in other studies such as Hovorka *et al.* (2004) where the models with closed boundaries experienced the greatest pressure buildup. This situation, of a storage site with closed boundaries on all sides, is likely to be unrealistic for storage in a saline aquifer. Further data collection from the site should investigate how thick the storage site is, as well as ascertaining the nature of the base boundary of the storage site as these two factors appear to have the greatest influence on pressure buildup at this site.

The thickness of the Rotliegend at the CCC prospect could be better estimated if a well were drilled which completely penetrated the Rotliegend in the vicinty of the CCC prospect and reached the unit

beneath. The collection of 3D seismic data which could be tied to this well would allow a much better estimate of the reservoir geometry. Hence, confidence in estimates of pressure buildup and plume migration modelled using this data would be increased.

Increasing the permeability of the storage formation independently of porosity of the storage formation reduces the pressure buildup seen at the top of the model (s01a, s01b4, s01c2). This finding is similar to the results of Chadwick *et al.* (2009a) who showed that near-field pressure (within a 2.5 m radius of the injection well) is inversely proportional to permeability. Increasing storage formation porosity independently of permeability leads to slightly higher pressure at the top of the model (s01a, s01a5). When both porosity and permeability are varied together, the models with higher porosity and permeability exhibit lower pressure buildup (s01a, s01b, s01c).

Reducing the porosity of the storage site substantially increases the plume diameter at the top of the storage site, with the largest plume diameter observed for the model with the lowest porosity. This is because the same amount of CO_2 has to spread out further in a low porosity formation in order to find enough pore space to be accommodated. Increasing the permeability of the storage site without changing the porosity results in the plume diameter increasing. This result is supported by the findings of Han *et al.* (2010) who showed that a larger area of the storage site is swept by CO_2 when the formation permeability is increased. Similarly Jahangiri & Zhang (2011) found that the overall plume spread in all directions is increased when formation permeability is higher. Han et al. (2010) also showed an increase in movement of CO2 through the reservoir for lower permeability ratio (k_v / k_h) which is likely to be the case for this reservoir although the permeability ratio has been kept constant in our simulations.

Decreasing porosity and permeability together results in a larger plume diameter in our models at the end of the simulation. For sandstones there is generally a strong positive correlation between porosity and permeability and therefore porosity and permeability should be varied together. The minimum permeability used in our models is higher than the permeability you would expect for a reservoir with the corresponding minimum porosity (Glennie 1998). If the permeability was lower it is likely that the plume diameter would be decreased and the pressure buildup increased. It will be necessary then to have a better constraint on the relationship between porosity and permeability in the reservoir in order to better predict the plume diameter.

The porosity and permeability values used in the most likely case are much closer to the values of porosity and corresponding permeability that you would expect for Rotliegend Sandstone. The plume diameter for the most likely case is within the CCC Prospect at the end of 120 years. However, it is close to the edge of the CCC prospect and would probably migrate past the spill point after 120 years. The two main ways to stop this happening would be to fill the CCC prospect more effectively and to increase dissolution and residual trapping within the reservoir. The CCC prospect could be more effectively filled if the CO_2 were injected using multiple wells or a horizontal well which could spread the CO_2 out over the whole area of the trap.

Ideally the porosity and permeability relationship in the reservoir could be investigated by collecting and analysing well logs and core data at the site. Correlation of similar facies across multiple locations throughout the site would allow a much more thorough understanding of the spatial distribution of differing porosities and permeabilities. Subsequent modelling using the data would provide a more detailed estimate of potential CO_2 migration. However, the nature of dynamic

585 modelling is such that if very detailed data were known it would still have to be upscaled somehow
586 and used to populate grid cells of approximately 10 m x 10 m. In consequence of this, whilst as much
587 porosity and permeability data as possible would be very useful, data on larger scales such as seismic
588 data, with one or two well ties, where porosity and permeability through the reservoir can be
589 deduced, would be more immediately applicable to building a dynamic model. Additionally, aside
590 from any issues relating to cost, it would be undesirable to have lots of wells drilled and core taken
591 from the site as this would increase the number of leakage pathways for CO_2 to escape to the
592 surface.

593 Dissolution and residual trapping have not been modelled in this study but they would reduce the
594 amount of free CO_2 within the plume and would therefore prevent the plume from spreading out so
595 far (Gasda *et al.* 2011). Some people have proposed ways of engineering the injection method to
596 increase these types of trapping. For example Qi et al. (2009) who suggested that injecting CO_2 with
597 brine and then injecting brine alone could increase residual trapping. The result of this would then
598 be an increase in dissolution trapping as the residually trapped CO_2 would dissolve in the brine
599 surrounding it.

600 Further modelling of the entire site up to and including the stratigraphic trap, would be useful to
601 determine the amount of CO_2 reaching the stratigraphic trap, and the time it would take to get there
602 if it leaks out of the CCC Prospect.

603 Looking at the effect of internal stratigraphic layering shows that pressure buildup at the top of the
604 model is reduced in the layered models. This is due to some CO_2 moving laterally beneath the
605 boundary between layers 1 and 2 away from the injection point. The resulting maximum pressure
606 buildup is reduced, as the CO_2 column above the injection point is thinned (Fig. 14). However, the
607 pressure increase affects a larger section of the reservoir because of the increased spread of CO_2
608 (Fig. 12). Core data from the site would give a much clearer indication of the layering present
609 beneath the CCC Prospect. Subsequent modelling using this information would provide a better
610 estimation of CO_2 migration at the site.

611 The effect of having a model with planar stratigraphy versus a model with irregular stratigraphy is
612 only apparent when comparing the layered models (s02a2, s07a). Here the influence of increased
613 stratigraphic relief leads to a more irregular plume shape with the plume extending further to the
614 east than in the flat layered model (Fig. 12(b)). A corresponding asymmetrical pressure profile can be
615 seen at the top of the model (Fig. 14(a)).

616 The irregular plume shape can be attributed to the movement of the CO_2 plume through the
617 reservoir from the injection point to the top of the storage site. After 10 years of injection, a small
618 amount of CO_2 has reached the top of the storage site above the injection point but some CO_2 has
619 spread along the layer boundary and pooled at an area of high stratigraphic relief, before rising to
620 the surface. The plume at top of the storage site has subsequently developed in an area slightly to
621 the east of the injection point, where there is a rise in the reservoir-caprock boundary, creating a
622 more irregular plume. Irregular plume shape, related to spreading of CO_2 along internal layering, has
623 been observed in modelling studies by Ghomian *et al.* (2008). It has also been inferred from seismic
624 data at Sleipner, where it can be seen that injected CO_2 is spreading beneath intraformational shale
625 layers, following areas of high relief of the stratigraphic boundaries (Arts *et al.* 2004).

In the homogeneous models and the flat layered model this has not happened as there is either no internal layering, or the layering is regular and contains no areas of high relief. This means that the CO_2 plume is still fairly regular in shape when it reaches the top of the storage site, leading to a correspondingly regular plume footprint.

Storage capacity

The simulations indicate that the site is likely to have a large enough storage capacity to accommodate injection of CO_2 at a rate of 2.5 Mt a^{-1} for 20 years. This leads to a total storage capacity of at least 50 Mt within the CCC Prospect. To put this into perspective, as of 2011, 12.7 Mt of CO_2 had been stored in the North Sea at Sleipner over 15 years (Statoil 2011). 50 Mt is between 0.01 and 0.025 % of the total amount of CO_2 required to be stored by the UK before 2050.

Pressure buildup in the case of the thin storage site with the closed boundary is very close to fracture pressure. If the storage site is thin with a closed boundary, it may be possible to prevent pressures reaching such high values by engineering the injection scheme in some way. For instance by injecting at a lower rate from multiple wells or by using a horizontal well which allows the CO_2 to be spread more evenly throughout the CCC Prospect. A large proportion of the CCC Prospect, to the north east, has not been filled. Further modelling should look at different injection schemes to determine the best way of filling the structure to maximise storage capacity and minimise pressure buildup.

Comparison of results with static capacity estimates

Hedley et al. (2013) used Monte-Carlo simulations to estimate static capacity at the site. Simulations were run for differing values of porosity, gross rock volume (volume of the CCC prospect), residual water saturation, maximum allowable pressure increase and efficiency factor. The efficiency factor is a factor related to the proportion of the reservoir which is likely to be swept by invading CO_2.

For each set of simulated variables the theoretical, open and closed capacities were estimated. The theoretical storage capacity is the pore volume of the reservoir, minus the residual water saturation, multiplied by density of CO_2 at the appropriate pressure and temperature conditions. The open storage capacity is the theoretical storage capacity multiplied by the efficiency factor. The closed storage capacity is the additional pore volume created by compressing the existing brine and rock within the reservoir up to the maximum allowable pressure buildup.

Statistics calculated from the results show that 80% of theoretical capacity estimates are in the range 42 Mt – 112 Mt. For open storage capacity estimates the range of results reduces to 7.59 Mt – 28 Mt. For closed storage capacity estimates 80% of the results were in the range 1.7 Mt – 3 Mt.

In comparison, dynamic modelling results indicate that for all models a storage capacity of 50 Mt can be achieved without exceeding fracture pressure. Albeit coming very close to fracture pressure for the closed thin system.

One reason for the large discrepancy between dynamic and static capacity estimates is that the static estimates only involve the volume of the CCC prospect down to the depth of the spill point. In the dynamic simulations there is CO_2 within the reservoir below the depth of the spill point. Once this has migrated above the spill point it is possible that the CO_2 will flow laterally past the spill point and leak from the CCC prospect, thereby reducing the modelled storage capacity. However, a large

volume of the CCC prospect to the north east has not been filled and it is more likely that CO_2 will migrate up dip to the north east and fill the rest of the CCC prospect before moving down dip past the spill point.

The presence of reservoir below the spill point will also have an effect on the capacity estimates for a closed aquifer. For capacity estimates relating to closed aquifers the only available pore space which can contain CO_2 is the additional pore space created by the compression of the brine and rock within the CCC prospect. This essentially assumes an impermeable layer directly below the CCC prospect at the level of the spill point. As the reservoir is likely to extend below the spill point the compressibility of the brine and rock below the CCC prospect must also be taken into account, increasing the extra pore space available to store CO_2.

Static capacity estimates for an open aquifer include a factor related to the sweep efficency of the aquifer. Sweep efficiency can be reduced by small scale permeability variations within the reservoir which lead to preferential flow of CO_2 through areas with higher permeability. Sweep efficiency can also be reduced by larger scale permeability variations in the reservoir related to the net to gross ratio of the reservoir rocks. Additionally, sweep efficiency can be related to the geometry of the stratigraphic layers and the tendency of the buoyant CO_2 to flow updip when it reaches a layer of lower permeability. This may cause channelling of the CO_2 along areas of high relief (e.g. Arts *et al.* 2004).

The dynamic simulations do not include small scale permeability variations due to heterogeneities in the sandstones or values of net to gross. Therefore they are likely to overestimate sweep efficency in the reservoir.

Static capacity estimates provide a way to quickly model many variations in reservoir parameters. However, there is a large discrepancy between the storage capacities predicted by the static models and those predicted by the dynamic models. This is primarily due to the fairly restrictive assumptions involved in the static capacity estimates. For instance the assumption of brine compressibility only within the trap in the case of a closed system is likely to be unrealistic in this case as we know the reservoir extends below the CCC prospect. Additionally the sweep efficiency factors used to estimate the open capacity of the trap are difficult to quantify without carrying out some form of dynamic modelling as well.

Comparison of results with analytical solutions for plume diameter and pressure buildup

Mathias et al. (2011) derived an analytical solution for calculating plume diameter and pressure buildup assuming vertical equilibrium. The analytical solution assumes that the side and base boundaries of the reservoir are impermeable.

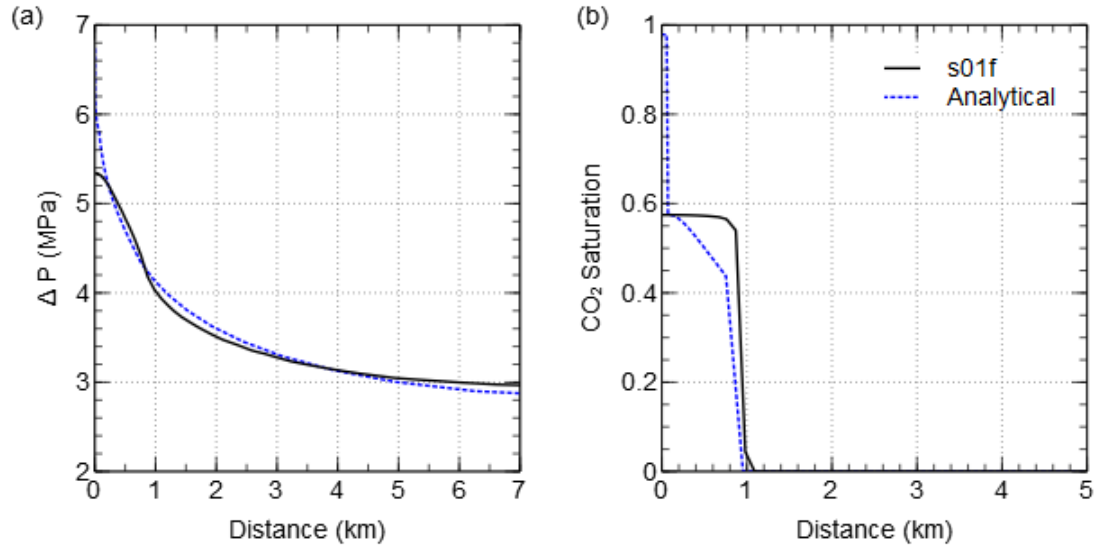

699

700 ***Fig. 15*** *Comparison of results of dynamic modelling from this study with the analytical solution of*
701 *Mathias et al. (2011). Reservoir is 320 m thick, injection well is at 0km* ***(a)*** *Change in presure.* ***(b)*** *CO2*
702 *saturation.*

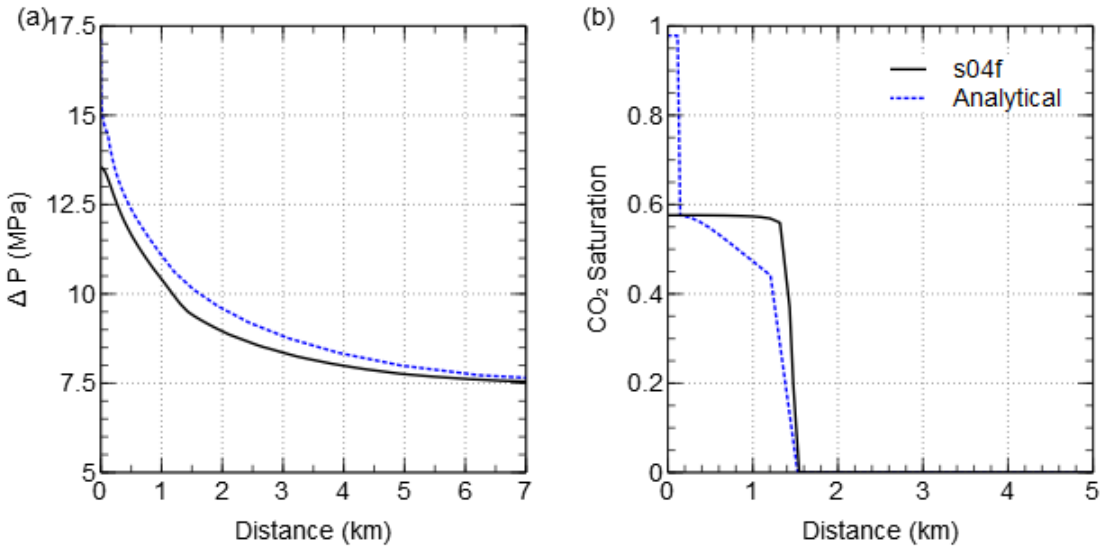

703

704 ***Fig. 16*** *Comparison of results of dynamic modelling from this study with the analytical solution of*
705 *Mathias et al. (2011). Reservoir is 320 m thick, injection well is at 0km* ***(a)*** *Change in presure.* ***(b)*** *CO2*
706 *saturation.*

707

708 Figs. 15 & 16 show the comparison of the analytical solution with the corresponding dynamic
709 solution for a reservoir thickness of 320 m and 120 m respectively. For both cases the pressure
710 buildup predicted by the analytical model is slightly higher directly above the injection point. The
711 plume diameters predicted by both models are very similar in both cases. The analytical model also

predicts a value for CO_2 saturation around the injection point which is higher that one minus the residual water saturation. This is due to the analytical solution modelling the dryout front, behind which the residual water has all dissolved into the CO_2 stream. The dynamic models also display this behaviour around the injection point but not at the surface where the results in Figs. 15 & 16 are taken from.

It can be seen that the analytical solutions provide very similar results to the dynamic models in certain situations. However, the main limitation is the fact that the analytical solutions can only be used to model certain situations i.e. where the storage site is surrounded by impermeable boundaries and where there is no internal heterogeneity.

Choice of dynamic modelling method

Using a full 3D numerical model has allowed us to produce results for storage capacity, pressure buildup and plume migration which include both the effects of vertical heterogeneity within the storage site and the geometry of the storage site. Using other dynamic modelling methods (e.g. streamline, vertical equilibrium etc.) would also give us indications of storage capacity, pressure buildup and plume migration. However, the large pressure change due to injection was considered unsuitable to be dealt with using streamline simulations. Additionally, the need to account for vertical layering and permeability anisotropy rendered vertical equilibrium modelling inappropriate. We have found that the combined presence of internal stratigraphic layering and stratigraphic relief has a noticeable impact on plume migration. Although we are not able to confidently predict plume migration at this stage, due to uncertainties in the input data, our modelling work indicates that the presence and properties of any stratigraphic layers in the storage site and the relief of potential layers are major influences on plume migration at the site. This supports the findings of several other case studies (e.g. Arts *et al.* 2004; Hovorka *et al.* 2004; Zhou *et al.* 2010). Therefore when entering the next stage of the project, more data should be collected regarding internal porosity and permeability variations within the reservoir and the stratigraphic relief of the site to facilitate more accurate modelling of CO_2 migration.

Conclusions

In this study we have created a preliminary dynamic model of a potential CO_2 storage site, within a deep saline formation, of the Rotliegend sandstones of the UK North Sea. Model properties have been derived from a limited set of primary data from the site, and from literature and well log data from nearby locations.

Our modelling results indicate that the site can store ~2.5 Mt a^{-1} of CO_2 over a period of 20 years without injected CO_2 reaching the containment spill point or the pressure exceeding the caprock fracture pressure, for up to 100 years after injection. A large section of the CCC structure has not been filled

The main controls on pressure buildup are the nature of the base boundary of the storage reservoir and the thickness of reservoir at the storage site. The main controls on plume diameter are the porosity, permeability and permeability anisotropy ratio of the formation.

The major uncertainties at the site are the properties of the unit beneath the Rotliegend at the location of the CCC Prospect and the thickness of the Rotliegend at the CCC Prospect. Further data

collection, such as the acquisition of a 3D seismic data set, tied to well data within the storage site, would assist in improving our understanding of these two parameters.

A thorough understanding of the porosity and permeability structure within the storage site would allow a much better estimate of plume migration pathways and plume diameter. To facilitate this more well and core data should be collected in the vicinity of the storage site. A compromise needs to be made between maximising the number of wells which can be drilled at the site and minimising the man-made leakage pathways for CO_2. Furthermore, it should be noted that for the purpose of dynamic modelling, data regarding small scale porosity and permeability variations (i.e. < 10 m resolution) will have to be scaled up and aggregated using a methodology similar to that described in this work, in order to populate a dynamic model. As a consequence, the acquisition of a high resolution seismic dataset in conjunction with a small number of well and core datasets would be more useful for building a dynamic model, than, for instance, collecting lots of core data without finding out any more information regarding the geometry and boundaries of the storage site.

Overall, the site looks promising for CO_2 storage and warrants some further investigation. Modelling using more detailed information will improve estimates for plume migration and pressure buildup. These models can then be used to test ways of filling the structure more efficiently, for instance with different injection locations, numbers of wells, and injection rates, in order to maximise CO_2 storage capacity and minimise pressure buildup within the CCC Prospect.

A comparison between static and dynamic modelling of the site for CO_2 sequestration shows that generally the dynamic capacity estimates exceed the static capacity estimates. This mainly due to the assumptions required to calculate static capacity estimates which are not necessarily true and are not required for the dynamic modelling. Analytical estimates of pressure buildup and plume diameter are very quick to calculate and provide a close match with dynamic models for scenarios with closed boundaries however they are not suitable for modelling other situations such as a reservoir with open boundaries or internal heterogeneity.

3D, grid based, numerical modelling has been useful as it has allowed us to identify and prioritise factors which could have a strong influence on the behaviour of CO_2 at the site even though only limited site data is available. This information will dictate the planning of future site characterisation work.

The authors would like to thank Progressive Energy Ltd. and TGS-NOPEC for access to seismic data. The authors would also like thank David Noy for his assistance with TOUGH2.

References

Arts, R. 2004. Monitoring of CO_2 injected at Sleipner using time-lapse seismic data. *Energy*, **29**(9-10), 1383–1392, doi:10.1016/j.energy.2004.03.072

Bennion, D. B. & Bachu, S. 2006. Supercritical CO_2 and H_2S – Brine Drainage and Imbibition Relative Permeability Relationships for Intergranular Sandstone and Carbonate Formations. *Society of Petroleum Engineers Paper 99326.*

Bentham, M. 2006. An assessment of carbon sequestration potential in the UK – Southern North Sea case study. *Tyndall Centre for Climate Change Research Working Paper 85.*

Boait, F. C., White, N. J., Bickle, M. J., Chadwick, R. A., Neufeld, J. A. & Huppert, H. E. 2012. Spatial and temporal evolution of injected CO_2 at the Sleipner Field, North Sea. *Journal of Geophysical Research*, **117**(B3), 1–21, doi:10.1029/2011JB008603

Chadwick, R. A., Noy, D. J. & Holloway, S. 2009a. Flow processes and pressure evolution in aquifers during the injection of supercritical CO_2 as a greenhouse gas mitigation measure. *Petroleum Geoscience*, **15**(1), 59–73, doi:10.1144/1354-079309-793

Chadwick, R. A., Noy, D., Arts, R. & Eiken, O. 2009b. Latest time-lapse seismic data from Sleipner yield new insights into CO_2 plume development. *Energy Procedia*, **1**(1), 2103–2110, doi:10.1016/j.egypro.2009.01.274

Chasset, C., Jarsjö, J., Erlström, M., Cvetkovic, V. & Destouni, G. 2011. Scenario simulations of CO2 injection feasibility, plume migration and storage in a saline aquifer, Scania, Sweden. *International Journal of Greenhouse Gas Control*, **5**(5), 1303–1318, doi:10.1016/j.ijggc.2011.06.003

Cornford, C. 1990. Source Rocks and Hydrocarbons of the North Sea. In K W Glennie (Ed.), *Introduction to the Petroleum Geology of the North Sea* (Third., pp. 294–361). Blackwell Science Ltd.

DECC. 2012. CCS Roadmap. Department of Energy and Climate Change.

Doughty, C. 2007. Modeling geologic storage of carbon dioxide: Comparison of non-hysteretic and hysteretic characteristic curves. *Energy Conversion and Management*, **48**(6), 1768–1781, doi:10.1016/j.enconman.2007.01.022

Doughty, C. 2010. Investigation of CO_2 plume behavior for a large-scale pilot test of geologic carbon storage in a saline formation. *Transport in Porous Media*, **82**(1), 49–76, doi:10.1007/s11242-009-9396-z

Eigestad, G. T., Dahle, H. K., Hellevang, B., Riis, F., Johansen, W. T. & Øian, E. 2009. Geological modeling and simulation of CO_2 injection in the Johansen formation. *Computational Geosciences*, **13**(4), 435–450, doi:10.1007/s10596-009-9153-y

Gasda, S. E., Nordbotten, J. M. & Celia, M. A. 2009. Vertical equilibrium with sub-scale analytical methods for geological CO_2 sequestration. *Computational Geosciences*, **13**(4), 469–481, doi:10.1007/s10596-009-9138-x

Gasda, S. E., Nordbotten, J. M. & Celia, M. A. 2011. Vertically averaged approaches for CO_2 migration with solubility trapping. *Water Resources Research*, **47**(5), 1–14, doi:10.1029/2010WR009075

Ghomian, Y., Pope, G. & Sepehrnoori, K. 2008. Reservoir simulation of CO_2 sequestration pilot in Frio brine formation, USA Gulf Coast. *Energy*, **33**(7), 1055–1067, doi:10.1016/j.energy.2008.02.011

Glennie, K.W. 1983. Early Permian (Rotliegendes) palaeowinds of the north sea. *Sedimentary Geology*, **34**(2-3), 245–265. doi:10.1016/0037-0738(83)90088-X

Glennie, K.W., Higham, J. & Stemmerik, L. 2003. Permian. In D. Evans, C. Graham, A. Armour, & P. Bathurst (Eds.), *The Millennium Atlas: petroleum geology of the central and northern North Sea.* (pp. 91–103). London: Geological Society of London.

827 Han, W. S., Lee, S.-Y., Lu, C. & McPherson, B. J. 2010. Effects of permeability on CO_2 trapping
828 mechanisms and buoyancy-driven CO_2 migration in saline formations. *Water Resources Research*,
829 **46**(7), 1–20, doi:10.1029/2009WR007850

830 Hatzignatiou, D. G., Riis, F., Berenblyum, R., Hladik, V., Lojka, R. & Francu, J. 2011. Screening and
831 evaluation of a saline aquifer for CO_2 storage: Central Bohemian Basin, Czech Republic. *International*
832 *Journal of Greenhouse Gas Control*, **5**(6), 1429–1442, doi:10.1016/j.ijggc.2011.07.013

833 Heinemann, N., Wilkinson, M., Pickup, G. E., Haszeldine, R. S. & Cutler, N. a. 2012. CO_2 storage in the
834 offshore UK Bunter Sandstone Formation. *International Journal of Greenhouse Gas Control*, **6**, 210–
835 219, doi:10.1016/j.ijggc.2011.11.002

836 Heward, A. P. 1991. Inside Auk - The anatomy of an eolian oil reservoir. In A. D. Miall & N. Tyler
837 (Eds.), The Three-Dimensional Facies Architecture of Terrigenous Clastic Sediments and Its
838 Implications for Hydrocarbon Discovery and Recovery (pp. 44–56), doi:10.2110/csp.91.03.0044

839 Heward, A. P., Schofield, P. & Gluyas, J. G. 2003. The Rotliegend reservoir in Block 30/24, UK Central
840 North Sea: including the Argyll (renamed Ardmore) and Innes fields. *Petroleum Geoscience*, **9**(4),
841 295–307, doi:10.1144/1354-079303-578

842 Hovorka, S. D., Doughty, C., Benson, S. M., Pruess, K. & Knox, P. R. 2004. The impact of geological
843 heterogeneity on CO_2 storage in brine formations: a case study from the Texas Gulf Coast.
844 *Geological Society, London, Special Publications*, **233**(1), 147–163,
845 doi:10.1144/GSL.SP.2004.233.01.10

846 IPCC. 2005. Carbon Dioxide Capture and Storage. (B. Metz, O. Davidson, H. de Coninck, M. Loos, & L.
847 Meyer, Eds.). Cambridge University Press.

848 Jahangiri, H. R. & Zhang, D. 2011. Effect of spatial heterogeneity on plume distribution and dilution
849 during CO_2 sequestration. *International Journal of Greenhouse Gas Control*, **5**(2), 281–293,
850 doi:10.1016/j.ijggc.2010.10.003

851 Jalalh, A. A. 2006. Compressibility of porous rocks: Part II. New relationships. *Acta Geophysica*, **54**(4),
852 399–412, doi:10.2478/s11600-006-0029-4

853 Jin, M., Pickup, G., Mackay, E., Todd, A., Monaghan, A., Survey, B. G. & Naylor, M. 2010. Static and
854 Dynamic Estimates of CO_2 Storage Capacity in Two Saline Formations in the UK. *Society of Petroleum*
855 *Engineers Paper 131609.*

856 Mathias, S. A., Gluyas, J. G., Oldenburg, C. M. & Tsang, C.-F. 2010. Analytical solution for Joule–
857 Thomson cooling during CO_2 geo-sequestration in depleted oil and gas reservoirs. *International*
858 *Journal of Greenhouse Gas Control*, **4**(5), 806–810, doi:10.1016/j.ijggc.2010.05.008

859 Mathias, S. A., González Martínez de Miguel, G. J., Thatcher, K. E. & Zimmerman, R. W. 2011.
860 Pressure Buildup During CO_2 Injection into a Closed Brine Aquifer. *Transport in Porous Media*, **89**(3),
861 383–397, doi:10.1007/s11242-011-9776-z

862 Mathias, S. A., Hardisty, P. E., Trudell, M. R. & Zimmerman, R. W. 2008. Approximate Solutions for
863 Pressure Buildup During CO_2 Injection in Brine Aquifers. *Transport in Porous Media*, **79**(2), 265–284,
864 doi:10.1007/s11242-008-9316-7

865 Møll Nilsen, H., Herrera, P. A., Ashraf, M., Ligaarden, I., Iding, M., Hermanrud, C., Lie, K.-A., et al.
866 2011. Field-case simulation of CO_2 -plume migration using vertical-equilibrium models. *Energy*
867 *Procedia*, **4**, 3801–3808, doi:10.1016/j.egypro.2011.02.315

868 Narasimhan, T. N. & Witherspoon, P. A. 1976. An Integrated Finite Difference Method for Analyzing
869 Fluid Flow. *Water Resources Research*, **12**(1), 57–64.

870 Nordbotten, J. M., Celia, M. A. & Bachu, S. 2005. Injection and Storage of CO_2 in Deep Saline
871 Aquifers: Analytical Solution for CO_2 Plume Evolution During Injection. *Transport in Porous Media*,
872 **58**(3), 339–360, doi:10.1007/s11242-004-0670-9

873 Noy, D. J., Holloway, S., Chadwick, R. A., Williams, J. D. O., Hannis, S. A. & Lahann, R. W. 2012.
874 Modelling large-scale carbon dioxide injection into the Bunter Sandstone in the UK Southern North
875 Sea. *International Journal of Greenhouse Gas Control*, **9**, 220–233, doi:10.1016/j.ijggc.2012.03.011

876 Obi, E. I. & Blunt, M. J. 2006. Streamline-based simulation of carbon dioxide storage in a North Sea
877 aquifer. *Water Resources Research*, **42**(3), doi:10.1029/2004WR003347

878 Oldenburg, C. 2007. Joule-Thomson cooling due to CO_2 injection into natural gas reservoirs. *Energy*
879 *Conversion and Management*, **48**(6), 1808–1815, doi:10.1016/j.enconman.2007.01.010

880 Pacala, S. & Socolow, R. 2004. Stabilization wedges: solving the climate problem for the next 50
881 years with current technologies. *Science (New York, N.Y.)*, **305**(5686), 968–72,
882 doi:10.1126/science.1100103

883 Pruess, K. 2005. ECO2N: A TOUGH2 Fluid Property Module for Mixtures of Water, NaCl, and CO_2.
884 *Lawrence Berkeley National Laboratory Report* **LBNL-57952**.

885 Pruess, K., García, J., Kovscek, T., Oldenburg, C., Rutqvist, J., Steefel, C. & Xu, T. 2004. Code
886 intercomparison builds confidence in numerical simulation models for geologic disposal of CO_2.
887 *Energy*, **29**, 1431–1444, doi:10.1016/j.energy.2004.03.077

888 Pruess, K., Oldenburg, C. & Moridis, G. 1999. TOUGH2 User's Guide, Version 2.0. *Lawrence Berkeley*
889 *National Laboratory Report* **LBNL-43134**.

890 Qi, R., Laforce, T. & Blunt, M. 2009. Design of carbon dioxide storage in aquifers. *International*
891 *Journal of Greenhouse Gas Control*, **3**(2), 195–205, doi:10.1016/j.ijggc.2008.08.004

892 Ringrose, P., Nordahl, K., & Wen, R. 2005. Vertical permeability estimation in heterolithic tidal deltaic
893 sandstones. *Petroleum Geoscience,* **11**(1), 29-36.

894 Schäfer, F., Walter, L., Class, H. & Müller, C. 2012. The regional pressure impact of CO_2 storage: a
895 showcase study from the North German Basin. *Environmental Earth Sciences*, **65**(7), 2037–2049,
896 doi:10.1007/s12665-011-1184-8

897 Selley, R. C. 1978. Porosity gradients in North Sea oil-bearing sandstones. *Journal of the Geological*
898 *Society*, **135**(1), 119–132, doi:10.1144/gsjgs.135.1.0119

899 Spycher, N., & Pruess, K. 2005. CO_2–H_2O mixtures in the geological sequestration of CO_2. II.
900 Partitioning in chloride brines at 12–100 ◦C and up to 600 bar. *Geochimica et Cosmochimica Acta,* **69**,
901 3309–3320, doi:10.1016/j.gca.2005.01.015

902 Statoil. 2011. Statoil Annual Report. World Wide Web Address:
903 http://www.statoil.com/AnnualReport2011

904 Taylor, J.. C. M. 1998. Upper Permian - Zechstein. In K. W. Glennie (Ed.), *Petroleum Geology of the*
905 *North Sea* (pp. 174 – 211). Oxford, UK: Blackwell Science Ltd., doi:10.1002/9781444313413

906 The European Union. 2009. Directive 2009/31/EC of the European Parliament and of the council.
907 *Official Journal of the European Union*.

908 Trewin, N. H., Fryberger, S. G. & Kreutz, H. 2003. The Auk Field, Block 30/16, UK North Sea. (J. G.
909 Gluyas & H. M. Hitchens, Eds.)*United Kingdom Oil and Gas Fields, Commemorative Millennium*
910 *Volume, Geological Society, London, Memoir*, **20**, 485–496.

911 Wyllie, M. R. J., Gregory, A. R., & Gardner, G. H. F. 1958. An experimental investigation of factors
912 affecting elastic wave velocities in porous media.*Geophysics*, *23*(3), 459-493.

913 Yamamoto, H. & Doughty, C. 2011. Investigation of gridding effects for numerical simulations of CO_2
914 geologic sequestration. *International Journal of Greenhouse Gas Control*,
915 doi:10.1016/j.ijggc.2011.02.007

916 Yamamoto, H., Zhang, K., Karasaki, K., Marui, A., Uehara, H. & Nishikawa, N. 2009. Numerical
917 investigation concerning the impact of CO_2 geologic storage on regional groundwater flow.
918 *International Journal of Greenhouse Gas Control*, **3**(5), 586–599, doi:10.1016/j.ijggc.2009.04.007

919 Yielding, G., Lykakis, N. & Underhill, J. R. 2011. The role of stratigraphic juxtaposition for seal
920 integrity in proven CO_2 fault-bound traps of the Southern North Sea. *Petroleum Geoscience*, **17**(2),
921 193–203, doi:10.1144/1354-0793/10-026

922 Zhang, K., Wu, Y., & Pruess, K. 2008. User ' s Guide for TOUGH2-MP - A Massively Parallel Version of
923 the TOUGH2 Code. *Lawrence Berkeley National Laboratory Report* **LBNL-315E**

924 Zhou, Q, Birkholzer, J., Tsang, C. & Rutqvist, J. 2008. A method for quick assessment of CO_2 storage
925 capacity in closed and semi-closed saline formations. *International Journal of Greenhouse Gas*
926 *Control*, **2**(4), 626–639, doi:10.1016/j.ijggc.2008.02.004

927 Zhou, Quanlin, Birkholzer, J. T., Mehnert, E., Lin, Y.-F. & Zhang, K. 2010. Modeling basin- and plume-
928 scale processes of CO_2 storage for full-scale deployment. *Ground water*, **48**(4), 494–514,
929 doi:10.1111/j.1745-6584.2009.00657.x

930